Journal of Structural Biology 197 (2017) 57–64

Contents lists available at ScienceDirect

Journal of Structural Biology

journal homepage: www.elsevier.com/locate/yjsbi

Mutual A domain interactions in the force sensing protein von Willebrand factor

Sandra Posch [a], Camilo Aponte-Santamaría [b], Richard Schwarzl [c], Andreas Karner [d], Matthias Radtke [c], Frauke Gräter [b], Tobias Obser [e], Gesa König [e], Maria A. Brehm [e], Hermann J. Gruber [a], Roland R. Netz [c], Carsten Baldauf [f], Reinhard Schneppenheim [e], Robert Tampé [g], Peter Hinterdorfer [a,d,*]

[a] Department of Applied Experimental Biophysics, Institute of Biophysics, Johannes Kepler University, Linz, Austria
[b] Molecular Biomechanics Group, Heidelberg Institute for Theoretical Studies, Heidelberg, Germany
[c] Department of Physics, FU Berlin, Berlin, Germany
[d] Center for Advanced Bioanalysis GmbH (CBL), Linz, Austria
[e] Department of Pediatric Hematology and Oncology, University Medical Center Hamburg-Eppendorf, Hamburg, Germany
[f] Theory Department, Fritz-Haber-Institut der Max-Planck-Gesellschaft, Berlin, Germany
[g] Institute of Biochemistry, Biocenter, Goethe-University Frankfurt, Frankfurt/Main, Germany

ARTICLE INFO

Article history:
Received 28 January 2016
Received in revised form 21 April 2016
Accepted 22 April 2016
Available online 23 April 2016

Keywords:
Atomic force microscopy
Single molecule force spectroscopy
Molecular dynamics simulation
Brownian dynamics simulation
von Willebrand factor
Primary hemostasis

ABSTRACT

The von Willebrand factor (VWF) is a glycoprotein in the blood that plays a central role in hemostasis. Among other functions, VWF is responsible for platelet adhesion at sites of injury via its A1 domain. Its adjacent VWF domain A2 exposes a cleavage site under shear to degrade long VWF fibers in order to prevent thrombosis. Recently, it has been shown that VWF A1/A2 interactions inhibit the binding of platelets to VWF domain A1 in a force-dependent manner prior to A2 cleavage. However, whether and how this interaction also takes place in longer VWF fragments as well as the strength of this interaction in the light of typical elongation forces imposed by the shear flow of blood remained elusive. Here, we addressed these questions by using single molecule force spectroscopy (SMFS), Brownian dynamics (BD), and molecular dynamics (MD) simulations. Our SMFS measurements demonstrate that the A2 domain has the ability to bind not only to single A1 domains but also to VWF A1A2 fragments. SMFS experiments of a mutant [A2] domain, containing a disulfide bond which stabilizes the domain against unfolding, enhanced A1 binding. This observation suggests that the mutant adopts a more stable conformation for binding to A1. We found intermolecular A1/A2 interactions to be preferred over intramolecular A1/A2 interactions. Our data are also consistent with the existence of two cooperatively acting binding sites for A2 in the A1 domain. Our SMFS measurements revealed a slip-bond behavior for the A1/A2 interaction and their lifetimes were estimated for forces acting on VWF multimers at physiological shear rates using BD simulations. Complementary fitting of AFM rupture forces in the MD simulation range adequately reproduced the force response of the A1/A2 complex spanning a wide range of loading rates. In conclusion, we here characterized the auto-inhibitory mechanism of the intramolecular A1/A2 bond as a shear dependent safeguard of VWF, which prevents the interaction of VWF with platelets.

1. Introduction

von Willebrand factor (VWF) is a huge multimeric protein that plays a key role in hemostasis. It triggers platelet adhesion in areas of vascular damage by binding to exposed sub-endothelial collagen to assist wound closure. In this process, VWF domain A1 is responsible for mediating platelet adhesion under flow in areas of vessel injury through the platelet glycoprotein Ibα (GPIbα) (Huizinga et al., 2002; Dumas et al., 2004; Lou and Zhu, 2008; Kim et al., 2010; Blenner et al., 2014). Domain A2 is unfolded under shear, whereupon it exposes a proteolytic site cleaved by the metalloprotease ADAMTS13 (Sadler, 2002; Baldauf et al., 2009; Chen et al., 2009; Zhang et al., 2009; Wu et al., 2010; Ying et al., 2010; Lippok et al., 2015). In the resting state, i.e. under low shear-stress conditions, VWF is incapable of binding platelets. This behavior has been associated with shielding of the GPIbα binding site by the adjacent units to A1, namely, the D′D3 domain

* Corresponding author at: Department of Applied Experimental Biophysics, Institute of Biophysics, Johannes Kepler University, Linz, Austria.
E-mail address: peter.hinterdorfer@jku.at (P. Hinterdorfer).

http://dx.doi.org/10.1016/j.jsb.2016.04.012
1047-8477/

(Ulrichts et al., 2006), the linker connecting D′D3 with A1 (Auton et al., 2012), and the A2 domain (Martin et al., 2007; Aponte-Santamaría et al., 2015). We recently found that the GPIbα-binding site in A1 becomes accessible by force-induced dissociation of the A1–A2 complex, whereas A2 mostly withstands unfolding under these forces and thereby remains protected against cleavage (Aponte-Santamaría et al., 2015). These insights have put forward new scenarios how VWF, in a shear-flow dependent manner, dynamically balances intra versus intermolecular A1A2 interactions, thereby guiding VWF self-assembly and activation. However, the inter- and intra-molecular forces and energies underlying dissociation and unfolding have remained elusive and the lifetime of these interactions have not been quantified nor compared to physiological shear regimes.

We addressed these issues by using single molecule force spectroscopy (SMFS), Brownian dynamics (BD) and molecular dynamics (MD) simulations. SMFS provided evidence for specific interactions between the important VWF domains A1 and A2. Binding activities, forces and bond stability were determined and put into context of physiological shear rates. Overall, our results underpin the strategy of a safeguarding mechanism in the competition between clot formation and VWF cleavage, depicted by the hierarchy of A1–A2 dissociation versus A2 unfolding forces in primary hemostasis.

2. Materials and methods

2.1. SMFS investigations

SMFS measurements were performed using a Pico SPM Plus setup (Agilent Technologies, Chandler, AZ, USA) under physiological conditions. Single VWF A-domains or VWF A domain constructs were either coupled to the AFM tip or to the sample surface. For SMFS experiments non-conductive Silicon Nitride MSCT tips (Brucker Corporation, MA, USA) with small spring constants (k = 0.03 N/m) were utilized. The actual spring constant was determined using the thermal noise method (Hutter and Bechhoefer, 1993).

2.2. Materials

All chemicals were used in the highest available purity. 3-Aminopropyl-triethoxy silane (APTES; Sigma Aldrich, Vienna, Austria) was distilled at low pressure and stored under argon in sealed crimp vials over silica gel (to avoid polymerization) at −20 °C. MilliQ (Millipore, Massachusetts, USA) purified water was used for all aqueous solutions. Triethylamine (TEA, Sigma Aldrich, Vienna, Austria) was stored under argon and in the dark to avoid amine oxidation. Chloroform was purchased from J.T. Baker (Griesheim, Germany), Argon and N_2 from Linde Gas GmbH (Stadl-Paura, Austria). HCl was purchased from Sigma Aldrich (Vienna, Austria). Ethylenediaminetetraacetic acid (EDTA) and Tris base were purchased from VWR International (Vienna, Austria), Hepes and $NiCl_2$ were obtained from Merck (Darmstadt Germany) and TCEP (tris(2-carboxyethyl)phosphine) hydrochloride from Molecular Probes, Invitrogen (Vienna, Austria). Disulfide-tris-NTA was generously provided by the Tampé lab, Biocenter, Frankfurt am Main, Germany. The heterobifunctional crosslinker maleimide-PEG_{27}-NHS was purchased from Polypure (Oslo, Norway). The cDNAs' coding for recombinant human VWF constructs containing the A1A2 (aa 1230–1672) construct, the single A1 (aa 1230–1463) and the single A2 (aa 1494–1672) were cloned into the mammalian expression vector pIRES neo2 (Schneppenheim et al., 2010). All VWF constructs are labeled with a His_6-tag. Mutations were inserted by site-directed mutagenesis employing the QuickChange kit (Stratagene). The vectors were used to transform Top10 super competent cells (Invitrogen) and sequenced. Plasmid purification was performed using the Endofree Plasmid Maxi Kit (QIAGEN). HEK293 cells were cultured in Dulbecco Modified Eagle Medium (DMEM, Invitrogen) with 10% [v/v] fetal bovine serum (Invitrogen) and 1% penicillin/streptavidin at 37 °C and 5% CO_2. These cells were transfected with the VWF vectors using Lipofectamine 2000 (Invitrogen) according to the manufacturer's instructions and recombinant expression of VWF variants was performed as previously described (Schneppenheim et al., 2001). His-tagged VWF domain constructs were purified employing the His-Pur Ni-NTA Resin (Thermo Fisher Scientific) according to the manufacturer's instruction for purification of His-tagged proteins using a gravity-flow column. Mica sheets were bought from Christine Groepl, Electron Microscopy (Tulln, Austria). For aqueous solutions, TBS buffer (50 mM Tris, 150 mM NaCl) and Hepes buffer (prepared from a 1 M solution of Hepes acid by adjustment of pH 7.5 or pH 9.6 – as stated in the text – with 20% NaOH) were used.

2.3. Tip chemistry for coupling VWF constructs

Proteins carrying a His_6-tag were coupled to the AFM tip (Verbelen et al., 2007) using the connector molecule tris-NTA and in the presence of $NiCl_2$. The protocols for the different steps of tip functionalization were optimized in our lab with respect to reproducibility, stability, and to the probability for binding on average one single ligand to the outer tip apex. They are available from the internet at http://www.jku.at/biophysics/content/e257042.

The first step was amino-functionalization of the tip surface: Commercial silicon-nitride cantilevers were washed with chloroform (3 × 5 min incubation) and dried in a gentle nitrogen gas stream directly before further treatment. The APTES functionalization was performed as described previously (Ebner et al., 2007): A desiccator (5 l) was flooded with argon gas to remove air and moisture. Then two small plastic trays (e.g. the lids of Eppendorf reaction vials) were placed inside the desiccator, 30 µl of APTES and 10 µl of triethylamine were separately pipetted into two trays, the AFM tips were placed nearby on a clean inert surface (e.g. Teflon) and the desiccator was closed. After 120 min of incubation, APTES and triethylamine were removed, the desiccator was again flooded with argon gas for 5 min, and the tips were left inside for two days in order to cure the APTES coating.

In a next step the coupling of the maleimide-PEG_{27}-NHS linker was performed: APTES-functionalized AFM tips were incubated in 0.5 ml of a 1 mg/ml solution of maleimide-PEG27-NHS in chloroform containing 0.5% (v/v) of TEA as base for two hours. Subsequently, the tips were rinsed in chloroform (3×) und dried in a gentle stream of nitrogen gas.

In the third step a tris-NTA function was coupled to the maleimide group on the outer end of the PEG chain. The cantilevers were then placed on parafilm in a polystyrene Petri dish. 100 µl disulfide-tris-NTA (1 mM in MilliQ water), 2 µl EDTA (100 mM, pH 7.5 in MilliQ water), 5 µl Hepes (1 M, pH 7.5), 2 µl TCEP hydrochloride (100 mM in MilliQ water) and 2.5 µl Hepes (prepared from a 1 M stock solution of Hepes acid by adjusting pH 9.6 with 20%NaOH) were mixed (final pH ∼ 7.5), pipetted on the tips, and incubated for two hours. Subsequently the tips were washed in TBS buffer (3 × 5 min).

In the last step the tris-NTA group was loaded with Ni^{2+} and His_6-tagged VWF proteins were bound: The cantilevers were again placed on parafilm in a polystyrene Petri dish and pre-loaded with 50 µl $NiCl_2$ (200 µM in TBS buffer, pH 7.5) for 5 min. Subsequently, 100 µl of the His_6-tagged protein was mixed with 4 µl 5 mM NiCl2 and incubated for 2 h. Finally, the tips were washed 3 times for

5 min in TBS. In the same way VWF constructs were also linked to APTES-coated mica sheets.

2.4. Statistical data evaluation

Interactions were probed by conducting force-distance-cycles (FDCs) at different loading rates r, i.e., at nine different velocities (50, 100, 200, 400, 600, 800, 1200, 2000 and 3000 nm/s). To gain reliable statistics, at least 1000 FDC were recorded at each pulling speed. The position of the tip relative to the surface was changed every 200 FDC, so as to statistically avoid position dependent artifacts. Unbinding events in the recorded FDC were marked with a polynomial fit. Binding events could be discerned from nonspecific adhesion by a characteristic parabolic force signal due to the elastic properties of the linkers. To additionally prove the specificity of the interactions, block experiments were performed. In this process, the ligand on the tip (e.g. VWF domain A1) was incubated with free receptors (e.g. VWF domains A2) in solution for two hours. The free receptors saturate the ligand on the tip and thus block the interaction between the ligand and the receptor on the sample surface. Thereafter, almost no specific interactions were observed in the FDC and the binding probability (BP), defined as the ratio between FDCs showing an unbinding event relative to the total number of FDCs, dramatically decreased (see Figs. 1 and 2 in Posch (2016)).

Probability density functions (pdf) of the measured forces were computed for each loading rate. A Gaussian distribution was fitted to the first peak of the pdf and forces within the interval $\mu \pm \sigma$ were used for further analysis (see Fig. 1(B) in Posch (2016)). The unbinding forces were plotted against the logarithm of the loading rate r, which is given by the product of the effective spring constant k_{eff} (slope at the rupture of an unbinding event, see Fig. 1(A) in Posch (2016)) and the pulling velocity v. The data points in this loading rate dependence plot (LRD) represent a single unbinding event each and were fitted with a single energy barrier binding model (Evans and Ritchie, 1997), using the maximum likelihood fitting routine (Wildling et al., 2012) to obtain the kinetic off-rate k_{off} and the width of the energy barrier x_β. In the interest of clarity, only the fits were shown and the data clouds were omitted. A typical example for such a data cloud is shown in Fig. 3 in Posch (2016). For better visualization of the bond stability, the bond lifetime τ (inverse of the kinetic off rate) was plotted. For the A1/A2 interactions (τ_0 = 1.5 s, x_β = 2.25 Å), a lifetime vs. unbinding force plot was generated by using the following relation:

$$\tau(F) = \tau_0 e^{\frac{-x_\beta F}{k_B T}} \quad (1)$$

where τ_0 denotes the lifetime of the bond without an applied external force. This plot allows to discriminate catch bond behavior from slip bond behavior of the studied interactions as presented in Rakshit et al. (2012).

2.5. BD simulations

BD simulations with hydrodynamic interactions (Ermak and McCammon, 1978) were performed in order to relate the single molecule force spectroscopy results from Eq. (1) to a physiological situation, where the VWF multimer is subject to shear flow. For this we used a coarse-grained bead spring model ((Posch, 2016), Eq. (1)) where each bead corresponds to a protomer of VWF with a reported radius of gyration of a = 30 nm (Singh et al., 2006). From simulations we extracted the tensile force profile, i.e. the elongation force between two adjacent beads along the chain ((Posch, 2016), Eq. (6)). This tensile force profile has been inserted into Eq. (1) to give an estimate of the lifetime of the A1/A2 complex. Hereby we assumed that the force acting on the A1/A2 complex inside each protomer is in the same range as the force acting along the multimer. The multimer was grafted onto the surface by fixing the position of one bead throughout the simulation (Fig. 3 inset). The simulation method has been described in previous publications (von Hansen et al., 2011; Radtke and Netz, 2015). The bead-bead cohesion strength was chosen to be $2k_BT$, since this value leads to a collapsed conformation of the VWF multimer in the untethered case (Schneider et al., 2007) and thus resembles the physiological situation of VWF in the bloodstream.

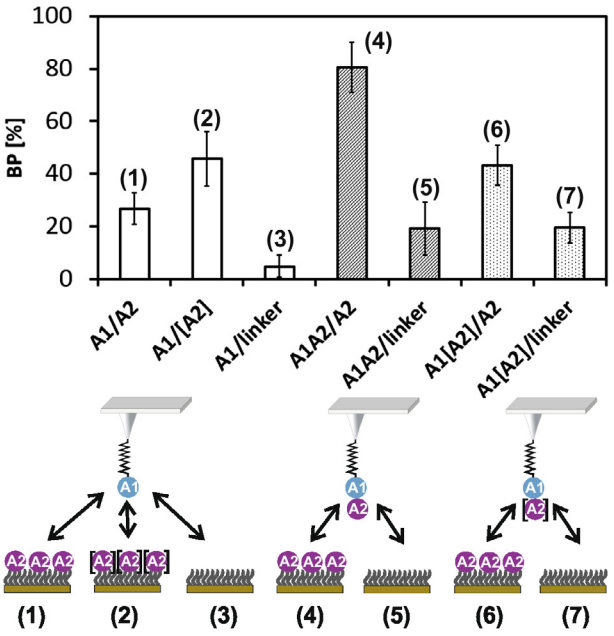

Fig. 1. BP of the interaction between VWF domains A1, the VWF A1A2 construct or the VWF A1[A2] construct and VWF domain A2 (1, 4, 6), as well as the VWF A1 domain and the disulfide-bridged [A2] mutant (2). Control measurements were carried out with no VWF A2 domains on the sample surface, but with the saturated linker (3, 5, 7). The VWF A domain constructs interacted specifically with the wt or mutant VWF A2 domains, which were immobilized on the sample support. Measurements were carried out using 4 different tips for each experiment.

2.6. MD simulations

Force-probe MD simulations displaying dissociation of the VWF A1-A2 complex were taken from our previous study (16 simulations starting from different inter-domain orientations) (Aponte-Santamaría et al., 2015). The N-terminus of A1 and the C-terminus of A2 were attached to virtual harmonic springs moving in opposing directions, thereby pulling away the two domains from each other. The force F acting on the complex was estimated as the average of the force acting on the termini. F was monitored during the simulations as a function of the separation between the springs. For each run, forces were smoothed, applying a Gaussian filter (σ equals 5% of the simulation length), and the maximum smoothed force was considered as the rupture force.

3. Results

3.1. Binding studies of VWF A1/A2 interactions

To study the interaction between domains A1 and A2 directly, AFM cantilevers were functionalized with the VWF A1 domain, and VWF A2 domains were immobilized on a sample surface. We also used a disulfide bridged A2 domain ([A2]) mutant (N1493C/C1670, aa1463-1672) coupled to the surface, in which the introduction of the disulfide bridge obstructs the mechanical unfolding

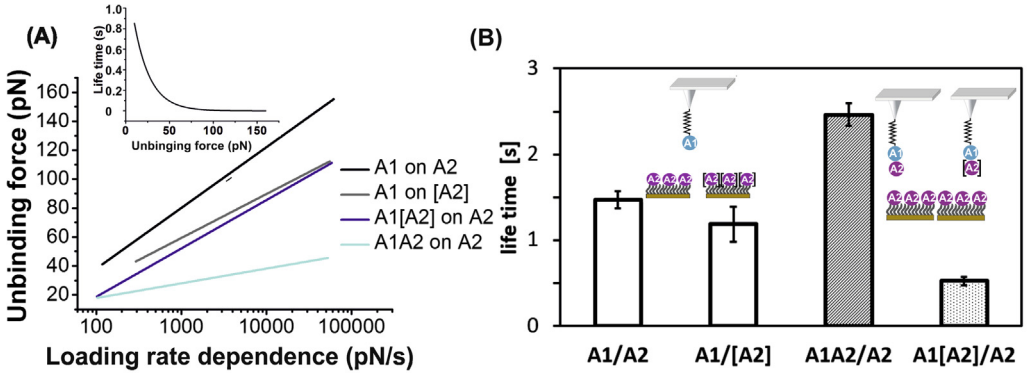

Fig. 2. (A) LRD plot: The black line shows the fit for the interaction measurement between VWF domain A1 and A2, the gray line for the A1/[A2] interaction, the dark blue line for A1[A2]/A2 interaction and the light blue line for A1A2/A2. Inset: The bond lifetime of the A1/A2 interaction was plotted as a function of the applied force. A clear slip bond behavior was found. (B) Corresponding lifetime values extrapolated to zero force of the four different interactions shown in (A). Inset: Experimental settings for the four different tip/surface combinations: A1/A2, A1/[A2], A1A2/A2, A1[A2]/A2.

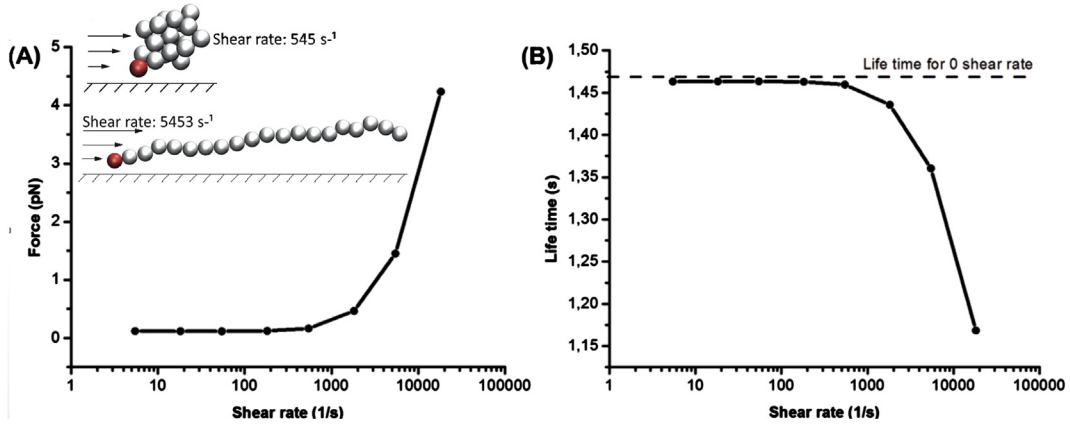

Fig. 3. In (A), the shear rate dependence of the force acting on the surface-grafted VWF A1/A2 complex is presented. (B) shows the lifetimes of the A1/A2 complex at different shear rates. The lifetime for zero shear rate, which we extracted from our AFM experiments, is illustrated with a dotted line.

of this domain and thus mimics the folded state of the A2 domain prior to unfolding by shear forces (Baldauf et al., 2009). In additional studies, tips were functionalized with either the wtVWF A1A2 or the A1[A2] construct. Overall, experiments were carried for four different tip/surface combinations: A1/A2, A1/[A2], A1A2/A2, A1[A2]/A2 (Fig. 1). We monitored the interaction forces between tip- and surface-bound molecules by consecutively recording force distance cycles (FDCs) (see Fig. 1 in Posch (2016)). Only a certain fraction of the FDCs contained molecular interaction signatures under the experimental conditions used. Experimental binding probabilities were monitored as a measure of binding activity. They were calculated as the ratio of FDCs containing a binding event over the total number recorded (at least 1000). To prove the specificity of binding, control experiments were carried out by a parallel experiment containing no A2 or [A2] domains, but only saturated linker molecules on the sample surface. They generally showed a much lower binding probability (Fig. 1). The specificity of the binding events was additionally tested by performing tip-blocking experiments. Hereby the VWF A1 tips were incubated with the corresponding A2 domain constructs (wt or mutant, c = 0.1 mg/ml, 2 h) to prevent the binding of the VWF A1 domain to the wt or mutant A2 domains on the sample surface. The remaining events correspond to unspecific adhesion. In all cases, the significant decrease of the BP suggests a high number of specific bindings (see Fig. 2 in Posch (2016)).

The binding probability of the interactions between VWF domains A1 and A2 was determined to be 27 ± 6%. The interactions between the VWF A1 domain and the bridged [A2] domains resulted in a significantly higher BP when compared to the wt system (BP = 46 ± 10%). This higher value could arise from the fact that the more rigid bridged [A2] domain is mostly in the proper conformation to bind to domain A1. The interaction between the VWF A1A2 construct bound to the AFM tip and the VWF A2 domains on the sample surface resulted in an unexpectedly large BP of about 80%. The high number of binding events for the wild-type A1A2 constructs indicates that free A2 domains are more prone to form an intermolecular bond with the A1A2 construct than with the isolated A1 domain, despite that the A1A2 construct contains a binding competitor A2 domain directly linked to the A1 domain.

The BP value reduced to about 43% when the A1A2 construct was replaced by the A1[A2] bridged construct at the AFM tip. This behavior can be attributed to a higher stability of the [A2] bridged domain on the tip, increasing the competition against the A2 domain on the surface for binding to A1. The fact that the VWF A1A2 or A1[A2] constructs show a high number of binding events to the VWF A2 surface suggests that the domains A2 or [A2] of VWF A1A2 or VWF A1[A2] constructs do not auto-inhibit domain A1 for platelet binding. Our data is consistent with our previous equilibrium MD simulations (Aponte-Santamaría et al., 2015) which showed a less pronounced blockage of the GPIbα binding site for

the linked A1A2 construct compared to the non-covalently linked A1 and A2 domains. Overall, our results support the notion that intermolecular A1/A2 interactions are preferred over intramolecular A1/A2 interactions, with the presence of the intra-molecular connecting linker attenuating the binding in the latter case. A1/A2 intermolecular interactions might be the basis for the organization of VWF strands at low-shear rates and of large VWF networks.

3.2. Unbinding forces and bond lifetimes associated with the A1/A2 interactions

VWF A1/A2 bond ruptures were measured by varying the dynamics of the FDC experiments, so as to achieve the bond lifetime of the interactions. For this purpose unbinding forces were determined in dependence of the loading rate (equivalent to the applied force load increase over time) for the four the different tip/surface combinations used above: A1/A2, A1/[A2], A1A2/A2, A1[A2]/A2 (Fig. 2(B)). In a loading rate range from 100 to 60,000 pN/s, unbinding forces to detach A1 from A2 were observed in the range from 50 to 140 pN. Thus, replacing A2 by the bridged mutant [A2] reduced the forces to 40–110 pN. Rupture forces were comparable when pushing/retracting A1[A2] from A2 on the surface (between 20 and 110 pN). Surprisingly, the interaction forces for A1A2/A2 were significantly lower (20–45 pN). The forces necessary to dissociate the A1/A2 complex are comparable to those to unfold A2. For comparison, the forces for A2 unfolding were previously determined to be multiples of 21 pN at loading rates of 22 and 90 pN/s (Ying et al., 2010), and 7–15 pN at loading rates ranging from about 3–700 pN/s (Zhang et al., 2009). For multimeric VWF unfolding, forces of 50 to 150 pN were observed at velocities of 100–10,000 nm/s (Wijeratne et al., 2013). For all the experiments mentioned here, lower loading rates were used in comparison to our study. Nevertheless, we recently showed that A2, if at all, only partially unfolds prior to A1/A2 dissociation under our experimental conditions (Aponte-Santamaría et al., 2015).

Fig. 2(A) presents the loading rate dependence (LRD) of the unbinding forces. In accord with Evan's single-energy barrier model (Merkel et al., 1999), we observed a linear rise in the unbinding force with respect to a logarithmically increasing loading rate (Figs. 2(A) and 3 in Posch (2016)). The lifetime of the bond at zero force (inverse of the kinetic off rate k_{off}) was extrapolated using a maximum likelihood approach (Wildling et al., 2012) from data fits (see Fig. 3 in Posch (2016)). The inset in Fig. 2(A) shows the force dependence of the bond lifetime, τ, of the VWF A1/A2 interaction derived from the LRD plot (Hinterdorfer and van Oijen, 2005) in Fig. 2. The exponential decrease is characteristic for a slip-bond type behavior (Marshall et al., 2003).

The lifetime for the different constructs (computed as inverse of the kinetic off rate k_{off}) is presented in Fig. 2(B). A lifetime of approximately 1.5 s was obtained for the A1/A2 interaction. This value was found to be similar to the unfolding of the A2 domain (~2 s) (Zhang et al., 2009). The bond lifetime slightly decreased by replacing A2 by the bridged A2 ([A2]), indicating a similar binding stability. The lifetime of the bond between the VWF A1A2 construct and WT A2 was 2.5 s and the equivalent disulfide bridged construct [A2] showed a bond lifetime of about 0.5 s. It seems that the VWF A1A2 construct does not only bind single A2 domains more often, but also significantly longer than the other constructs. These findings suggest a stabilizing mechanism for $A1/A2_{surface}$ binding by the neighboring A2 domain. The lower bond lifetime of the A1[A2] construct goes well in line with the observation of a decreased BP. It is very likely that [A2], as an "easy" intramolecular binding partner to A1, destabilizes the intermolecular A1/A2 interactions.

3.3. Tensile forces at physiological shear-rates from BD Simulation

We next investigated whether the forces and lifetimes measured from force-probing single-molecule studies were of relevance for physiological shear conditions imposed by blood flow. Mean tensile force profiles for physiological shear rates between 5 s^{-1} and 20,000 s^{-1} were extracted for a surface grafted multimer chain of 20 protomers corresponding to a total length of 1.14 μm (see Fig. 4 in Posch (2016)). These tensile force profiles show that for VWF attached to the vessel wall, the strongest elongation force along the multimer is the force between the surface-grafted protomer and the adjacent protomer. The tensile force acting between these two protomers in dependence on the shear rate is shown in Fig. 3A. We calculated the shear dependent estimated lifetime of the A1/A2 complex closest to the fixed end of the multimer by plugging the mean tensile force from BD simulations into the experimentally found relation from Eq. (1). We found estimated lifetimes of 1.46 s and 1.17 s at shear rates of 545 s^{-1} and 1817 s^{-1}, which are in the range of shear rates as they occur in venules and arterioles, respectively (Papaioannou and Stefanadis, 2005). Both physiologically relevant estimated lifetimes are close to the experimentally fitted lifetime at zero force τ_0 = 1.5 s (Fig. 2(B)).

3.4. Rupture forces from MD simulations

We investigated the force-response of the VWF A1–A2 complex at the molecular level through force-probe MD simulations (Fig. 4 (A, B)). Force-distance profiles were largely influenced by the inter-domain orientation, causing differences in their extension, number of peaks, and magnitude of the rupture force (Fig. 4(A)). For the applied loading-rate of $r = 8.3 \times 10^{10}$ pN/s, rupture forces were found to be in a range from 150 pN to 450 pN (Fig. 4(B)). Interestingly, large rupture forces were observed for orientations in which the β-sheet of the A2 domain aligned nearly parallel to the pulling axis, presumably offering large resistance to rupture. Furthermore, the simulation in which the A2 domain substantially unfolded displayed the largest rupture-force values: one of around 400 pN associated to the detachment of β6 from the core of the protein (peak at a distance of around 11 nm in Fig. 4(A)) and the other one corresponding to the dissociation of the complex (peak at a distance around 19 nm in Fig. 4(A)). This is consistent with our AFM experiments, which showed increased rupture forces for the A1/A2 construct (with A2 able to unfold) compared to the A1/[A2] bridged construct (with A2 unable to unfold).

Forces from AFM experiments and MD simulations also showed qualitative agreement between A1/A2 and A1/[A2] when extrapolating the AFM data to the higher loading-rates used in MD simulations (see detailed fitting analysis in Posch (2016), Figs. 4(C, D) and 5 in Posch (2016)). The BSK model using exclusively the AFM data led to unrealistic large values in the MD regime (Fig. 5(A, B) in Posch (2016)). This result stresses the difficulties of extrapolating the rupture forces from AFM to high loading-rate regimes (Rico et al., 2013). Including the MD data in the BSK fit, as a way of constraining its extent at large loading-rates, improved the fits and reduced the theoretical rupture forces to values close to the ones observed in the simulations (Fig. 4(C, D)). Both fitting schemes preserved the trend of large forces for the A1/A2 construct compared to A1/[A2] construct. The constrained BSK fit for the A1/A2 wild-type construct predicted rupture forces in the range of 700–1000 pN for a loading rate of 1012 pN/s (Fig. 4(C)). This range agrees with the values for the unfolding of A2 of around 800 pN (Interlandi et al., 2012) and 1000 pN (Baldauf et al., 2009), derived from simulations at similar loading rates using different force fields. Moreover, at MD regimes, force increments have been previ-

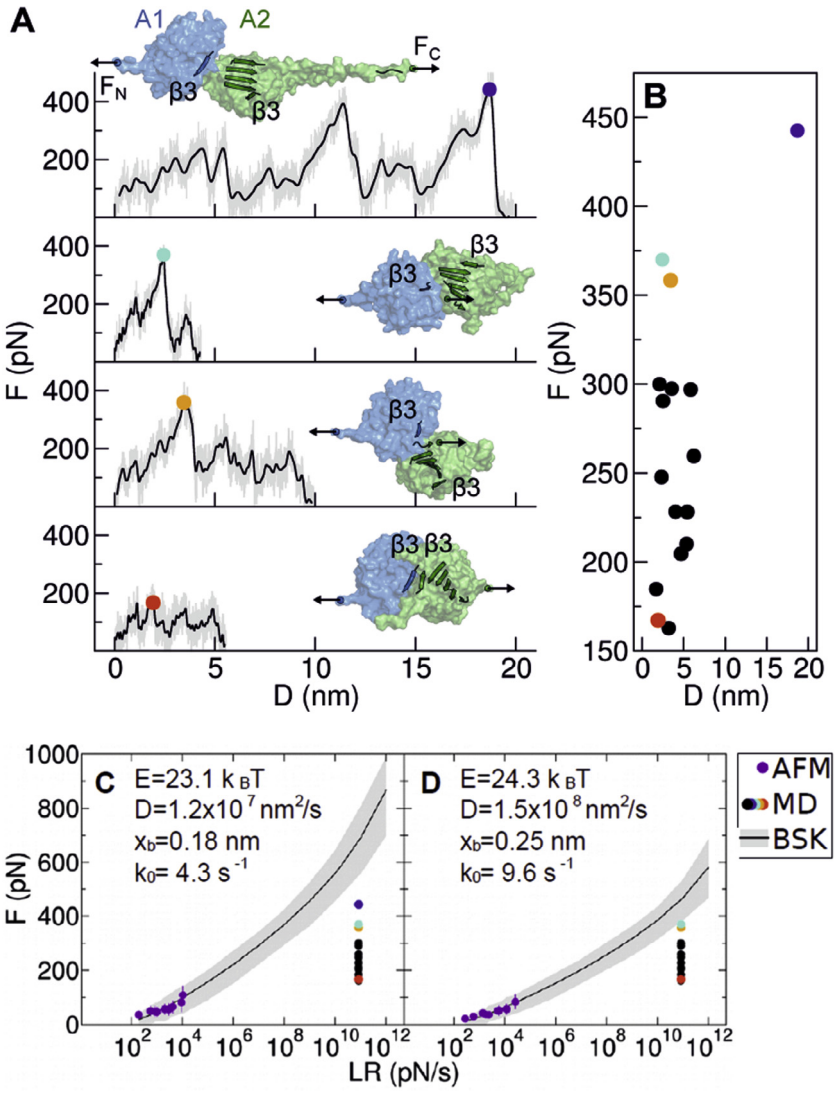

Fig. 4. Force response of the A1A2 complex during force-probe MD simulations. (A) Force-distance profiles recovered from four exemplary simulations starting from different inter-domain orientations. Raw data shown in gray and smoothed profiles in black. Highest peak after smoothing was considered as the rupture force (colored dot). Cartoons illustrate the conformation of the two domains at the moment of rupture. Protein domains are shown in surface representation. To highlight the different inter-domain orientations, the β3 strands of both domains are displayed in cartoon representation, as well as the β-sheet of the A2 domain. Termini where the force was exerted are shown as spheres. Force on the N-terminus (FN) and on the C-terminus of the A2 domain (FC) are sketched with the black arrows. (B) Maximum force (rupture force) as a function of the distance recovered from 16 different simulations. Points in color correspond to the peaks shown in (A).In (C) and (D) rupture forces of the A1-A2 complex as a function of the applied loading rate, for the A1-A2 wild-type complex A1/A2 (C) and for its bridged mutant A1/[A2] (D). Forces measured by AFM (average ± stdev) and computed from MD simulations are shown with dots. For the A1/[A2] bridged construct, the largest MD rupture force, observed upon unfolding of the A2 domain, was excluded. Forces were fitted using the Bullerjahn, Sturm and Kroy (BSK) model (Bullerjahn et al., 2014). Fitting was carried out constrained including MD data (C and D). Average (solid line) and the 95% confidence interval (gray area) are shown. (E, D, x_b, k_0) fitting parameters are indicated in each panel. The unconstrained fitting is shown in Fig. 5 in Posch (2016).

ously found to be of the order of hundreds of pN upon ten-fold increase in the loading-rate (Lee et al., 2009; Sotomayor et al., 2012; Rico et al., 2013). The constrained BSK model predicts such increments also for the A1/A2 dissociation. Taken together, our fits suggest that the constrained BSK model adequately reproduces the force-response of the A1–A2 complex spanning a large range of loading rates, covering the AFM data and predicting the forces at rupture to be observed in force-probe MD simulations. Large rupture force values derived from our previous simulations (Aponte-Santamaría et al., 2015) are close to that range but overall tend to be underestimated, presumably due to not fully stable conformations adopted by the complex before pulling. Nevertheless, their relative differences are consistent with larger rupture forces observed exclusively for the native construct in which the A2 domain is able to unfold. We note that MD forces were overall lower than extrapolated AFM forces. This can be explained by the fact that our simulations started from A1/A2 complexes predicted from docking and thus are likely to underestimate unbinding forces.

4. Summary

Here, we used a combined approach utilizing single molecule force spectroscopy, Brownian dynamics and molecular dynamics simulations to expand the knowledge about the force-response of the VWF A1/A2 protein/protein interaction. These interactions were reported to be the main player in a new auto-inhibition mechanism, which explains the inactivation of VWF under equilibrium conditions and the shear-sensitive growth of blood coagulates. In our study we probed the interaction strength and the binding activity between the VWF A1 and A2 domains at the single

molecule level utilizing single molecule force spectroscopy (SMFS). We investigated the effect of a disulfide bridge that obstructs the mechanical unfolding of A2 ([A2]), as well as the impact of a second A2 domain on A1/A2 binding.

Forces to rupture the VWF A1–A2 complex between 50 and 140 pN were observed for a wide range of loading rates ranging from 100 to 60,000 pN/s. Such data revealed specific recognition, underlying a slip bond behavior with a bond life time of ~1.5 s. SMFS experiments resulted in a higher number of specific binding events of A1 to the [A2] mutant when compared to wt A2. This indicates the disulfide bond A2 domain adopts a more proper conformation to bind domain A1. This is in line with the higher compactness of bridged [A2]-VWF multimer mutants compared to wild-type as observed in gel electrophoresis (Baldauf et al., 2009). No significant difference in bond life-time could be observed between these two systems. Thus we suggest that even though the binding of the VWF domain A1 shows a higher probability to bind [A2], the bond formed between A1 and the wt or the mutant [A2] domain is similarly stable.

The A2 domain of the VWF A1A2 construct does not appear to auto-inhibit the A1 domain in the construct, as a high number of binding events were observed between this construct and free A2 domains. Thus, our data imply that single A2 domains are able to bind not only to isolated A1 domains, as observed previously (Martin et al., 2007; Aponte-Santamaría et al., 2015), but also to longer VWF fragments containing A1. This further expands the extent of this interaction to more realistic functional VWF multi A-domain fragments. A1A2/A2 interactions showed a significantly higher binding probability and bond life-time, compared to the other constructs, but less force was needed to separate the A1A2 construct from domain A2. In contrast to the wt system, the A1 [A2] construct showed a lower binding probability, as well as a lower bond life-time. This behavior can be attributed to a higher degree of competition for binding between the intramolecular [A2] domain and the intermolecular A2 domain. Based on these competitive binding experiments, we speculate that the linker between A1 and A2, the structure of which is unknown, interferes with a direct intramolecular interaction, leading to a preference for intermolecular A1/A2 interactions. Another possible explanation could be a second binding site for A2 in domain A1, resulting in a positive cooperative binding behavior.

Additional MD and BD simulations completed our scientific work. Fitting AFM and MD based rupture forces with a constrained model of Bullerjahn, Sturm and Kroy made it possible to combine AFM and MD data spanning a wide range of loading rates (10^2–10^{12} pN/s). Complementary BD simulations revealed the dependence between the forces and lifetimes acting on VWF multimers under different shear conditions. In summary, we find the force-induced dissociation of specific VWF A-domain interactions to be a key initial step of VWF activation for platelet under shear.

Acknowledgements

This study was supported by the DFG (Deutsche Forschungsgemeinschaft) within the Research group FOR1543: "Shear flow regulation of hemostasis – bridging the gap between nanomechanics and clinical presentation (SHENC)", the FWF (Austrian Science Fund) Project I 767-B11 to S.P. and P25844 to A.K., by the European Fund for Regional Development (EFRE, Regio 13) and by the Klaus Tschira Foundation (to F.G.). We thank Christian Rankl (Agilent, Linz) for his support in data evaluation, as well as Hermann Gruber (JKU, Linz) and Robert Tampé (Goethe-University Frankfurt) for providing cross linker. We acknowledge Sebastian Sturm and Jakob Thomas Bullerjahn for kindly providing the scripts for fitting the rupture force data at high loading rates and for helpful discussions.

Appendix A. Supplementary data

Supplementary data associated with this article can be found, in the online version, at http://dx.doi.org/10.1016/j.jsb.2016.04.012.

References

Aponte-Santamaría, C., Huck, V., Posch, S., Bronowska, A.K., Grässle, S., Brehm, M.A., Obser, T., Schneppenheim, R., Hinterdorfer, P., Schneider, S.W., 2015. Force-sensitive autoinhibition of the von Willebrand factor is mediated by interdomain interactions. Biophys. J. 108 (9), 2312–2321.

Auton, M., Sowa, K.E., Behymer, M., Cruz, M.A., 2012. N-terminal flanking region of A1 domain in von Willebrand factor stabilizes structure of A1A2A3 complex and modulates platelet activation under shear stress. J. Biol. Chem. 287 (18), 14579–14585.

Baldauf, C., Schneppenheim, R., Stacklies, W., Obser, T., Pieconka, A., Schneppenheim, S., Budde, U., Zhou, J., Gräter, F., 2009. Shear-induced unfolding activates von Willebrand factor A2 domain for proteolysis. J. Thromb. Haemost. 7 (12), 2096–2105.

Blenner, M.A., Dong, X., Springer, T.A., 2014. Structural basis of regulation of von Willebrand factor binding to glycoprotein Ib. J. Biol. Chem. 289 (9), 5565–5579.

Bullerjahn, J.T., Sturm, S., Kroy, K., 2014. Theory of rapid force spectroscopy. Nat. Commun. 5.

Chen, W., Lou, J., Zhu, C., 2009. Molecular dynamics simulated unfolding of von Willebrand factor A domains by force. Cell. Mol. Bioeng. 2 (1), 75–86.

Dumas, J.J., Kumar, R., McDonagh, T., Sullivan, F., Stahl, M.L., Somers, W.S., Mosyak, L., 2004. Crystal structure of the wild-type von Willebrand factor A1-glycoprotein Ibα complex reveals conformation differences with a complex bearing von Willebrand disease mutations. J. Biol. Chem. 279 (22), 23327–23334.

Ebner, A., Hinterdorfer, P., Gruber, H.J., 2007. Comparison of different aminofunctionalization strategies for attachment of single antibodies to AFM cantilevers. Ultramicroscopy 107 (10–11), 922–927.

Ermak, D.L., McCammon, J., 1978. Brownian dynamics with hydrodynamic interactions. J. Chem. Phys. 69 (4), 1352–1360.

Evans, E., Ritchie, K., 1997. Dynamic strength of molecular adhesion bonds. Biophys. J. 72 (4), 1541–1555.

Hinterdorfer, P., van Oijen, A., 2005. Handbook of Single-Molecule Biophysics. Springer, Dordrecht Heidelberg London New York.

Huizinga, E.G., Tsuji, S., Romijn, R.A., Schiphorst, M.E., de Groot, P.G., Sixma, J.J., Gros, P., 2002. Structures of glycoprotein Ibα and its complex with von Willebrand factor A1 domain. Science 297 (5584), 1176–1179.

Hutter, J.L., Bechhoefer, J., 1993. Calibration of atomic-force microscope tips. Rev. Sci. Instrum. 64 (7), 1868–1873.

Interlandi, G., Ling, M., Tu, A.Y., Chung, D.W., Thomas, W.E., 2012. Structural basis of type 2A von Willebrand disease investigated by molecular dynamics simulations and experiments. PloS one 7 (10), e45207.

Kim, J., Zhang, C.-Z., Zhang, X., Springer, T.A., 2010. A mechanically stabilized receptor-ligand flex-bond important in the vasculature. Nature 466 (7309), 992–995.

Lee, E.H., Hsin, J., Sotomayor, M., Comellas, G., Schulten, K., 2009. Discovery through the computational microscope. Structure 17 (10), 1295–1306.

Lippok, S., Radtke, M., Obser, T., Kleemeier, L., Schneppenheim, R., Budde, U., Netz, R. R., Rädler, J.O., 2015. Shear-induced unfolding and enzymatic cleavage of full-length VWF multimers. arXiv preprint arXiv:1512.05127.

Lou, J., Zhu, C., 2008. Flow induces loop-to-β-hairpin transition on the β-switch of platelet glycoprotein Ibα. Proc. Natl. Acad. Sci. 105 (37), 13847–13852.

Marshall, B.T., Long, M., Piper, J.W., Yago, T., McEver, R.P., Zhu, C., 2003. Direct observation of catch bonds involving cell-adhesion molecules. Nature 423 (6936), 190–193.

Martin, C., Morales, L., Cruz, M., 2007. Purified A2 domain of von Willebrand factor binds to the active conformation of von Willebrand factor and blocks the interaction with platelet glycoprotein Ibα. J. Thromb. Haemost. 5 (7), 1363–1370.

Merkel, R., Nassoy, P., Leung, A., Ritchie, K., Evans, E., 1999. Energy landscapes of receptor–ligand bonds explored with dynamic force spectroscopy. Nature 397 (6714), 50–53.

Papaioannou, T.G., Stefanadis, C., 2005. Vascular wall shear stress: basic principles and methods. Hellenic J. Cardiol. 46 (1), 9–15.

Posch, S., Aponte-Santamaría, C., Schwarzl, R., Karner, A., Radtke, M., Gräter, F., Obser, T., König, G., Brehm, M.A., Gruber, H.J, Netz, R.R., Baldauf, C., Schneppenheim, R., Tampé, R., Hinterdorfer, P., 2016. Single molecule force spectroscopy and BD- and MD simulations on the blood protein von Willebrand factor. J. Struct. Biol., Data in Brief, submitted, (Special Issue entitled From Molecular Forces to Cellular Function)

Radtke, M., Netz, R.R., 2015. Shear-enhanced adsorption of a homopolymeric globule mediated by surface catch bonds. Eur. Phys. J. E 38 (6), 1–11.

Rakshit, S., Zhang, Y., Manibog, K., Shafraz, O., Sivasankar, S., 2012. Ideal, catch, and slip bonds in cadherin adhesion. Proc. Natl. Acad. Sci. 109 (46), 18815–18820.

Rico, F., Gonzalez, L., Casuso, I., Puig-Vidal, M., Scheuring, S., 2013. High-speed force spectroscopy unfolds titin at the velocity of molecular dynamics simulations. Science 342 (6159), 741–743.

Sadler, J.E., 2002. A new name in thrombosis, ADAMTS13. Proc. Natl. Acad. Sci. 99 (18), 11552–11554.
Schneider, S., Nuschele, S., Wixforth, A., Gorzelanny, C., Alexander-Katz, A., Netz, R., Schneider, M., 2007. Shear-induced unfolding triggers adhesion of von Willebrand factor fibers. Proc. Natl. Acad. Sci. 104 (19), 7899–7903.
Schneppenheim, R., Budde, U., Obser, T., Brassard, J., Mainusch, K., Ruggeri, Z.M., Schneppenheim, S., Schwaab, R., Oldenburg, J., 2001. Expression and characterization of von Willebrand factor dimerization defects in different types of von Willebrand disease. Blood 97 (7), 2059–2066.
Schneppenheim, R., Michiels, J.J., Obser, T., Oyen, F., Pieconka, A., Schneppenheim, S., Will, K., Zieger, B., Budde, U., 2010. A cluster of mutations in the D3 domain of von Willebrand factor correlates with a distinct subgroup of von Willebrand disease: type 2A/IIE. Blood 115 (23), 4894–4901.
Singh, I., Shankaran, H., Beauharnois, M.E., Xiao, Z., Alexandridis, P., Neelamegham, S., 2006. Solution structure of human von Willebrand factor studied using small angle neutron scattering. J. Biol. Chem. 281 (50), 38266–38275.
Sotomayor, M., Weihofen, W.A., Gaudet, R., Corey, D.P., 2012. Structure of a force-conveying cadherin bond essential for inner-ear mechanotransduction. Nature 492 (7427), 128–132.
Ulrichts, H., Udvardy, M., Lenting, P.J., Pareyn, I., Vandeputte, N., Vanhoorelbeke, K., Deckmyn, H., 2006. Shielding of the A1 domain by the D′ D3 domains of von Willebrand factor modulates its interaction with platelet glycoprotein Ib-IX-V. J. Biol. Chem. 281 (8), 4699–4707.
Verbelen, C., Gruber, H.J., Dufrêne, Y.F., 2007. The NTA–His6 bond is strong enough for AFM single-molecular recognition studies. J. Mol. Recognit. 20 (6), 490–494.
von Hansen, Y., Hinczewski, M., Netz, R.R., 2011. Hydrodynamic screening near planar boundaries: effects on semiflexible polymer dynamics. J. Chem. Phys. 134 (23), 235102.
Wijeratne, S.S., Botello, E., Yeh, H.-C., Zhou, Z., Bergeron, A.L., Frey, E.W., Patel, J.M., Nolasco, L., Turner, N.A., Moake, J.L., 2013. Mechanical activation of a multimeric adhesive protein through domain conformational change. Phys. Rev. Lett. 110 (10), 108102.
Wildling, L., Rankl, C., Haselgrübler, T., Gruber, H.J., Holy, M., Newman, A.H., Zou, M.-F., Zhu, R., Freissmuth, M., Sitte, H.H., 2012. Probing binding pocket of serotonin transporter by single molecular force spectroscopy on living cells. J. Biol. Chem. 287 (1), 105–113.
Wu, T., Lin, J., Cruz, M.A., Dong, J.-F., Zhu, C., 2010. Force-induced cleavage of single VWFA1A2A3 tridomains by ADAMTS-13. Blood 115 (2), 370–378.
Ying, J., Ling, Y., Westfield, L.A., Sadler, J.E., Shao, J.-Y., 2010. Unfolding the A2 domain of von Willebrand factor with the optical trap. Biophys. J . 98 (8), 1685–1693.
Zhang, X., Halvorsen, K., Zhang, C.-Z., Wong, W.P., Springer, T.A., 2009. Mechanoenzymatic cleavage of the ultralarge vascular protein von Willebrand factor. Science 324 (5932), 1330–1334.